

---

# Generating images with recurrent adversarial networks

---

Daniel Jiwong Im<sup>1</sup>

Chris Dongjoo Kim<sup>2</sup>

Hui Jiang<sup>2</sup>

Roland Memisevic<sup>1</sup>

IMDANIEL@IRO.UMONTREAL.CA

KIMDON20@GMAIL.COM

HJ@CSE.YORKU.CA

MEMISEVR@IRO.UMONTREAL.CA

<sup>1</sup>Montreal Institute for Learning Algorithms, University of Montreal

<sup>2</sup>Department of Engineering and Computer Science, York University

## Abstract

Gatys et al. (2015) showed that optimizing pixels to match features in a convolutional network with respect to reference image features is a way to render images of high visual quality. We show that unrolling this gradient-based optimization yields a recurrent computation that creates images by incrementally adding onto a visual “canvas”. We propose a recurrent generative model inspired by this view, and show that it can be trained using adversarial training to generate very good image samples. We also propose a way to quantitatively compare adversarial networks by having the generators and discriminators of these networks compete against each other.

## 1. Introduction

Generating realistic-looking images has been a long-standing goal in machine learning. The early motivation for generating images was mainly as a diagnostic tool, based on the belief that a good generative model can count as evidence for the degree of “understanding” that a model has of the visual world (see, example, (Hinton et al., 2006), (Hyvriinen et al., 2009), or (Ranzato et al., 2013) and references in these). More recently, due to immense quality improvements over the last two years (for example, (Gregor et al., 2015; Denton et al., 2015; Radford et al., 2015; Gatys et al., 2015)), and the successes of discriminative modeling overall, image generation has become a goal on its own, with industrial applications within close reach.

Currently, most common image generation models can be roughly categorized into two classes: The first are based on probabilistic generative models, such as the variational autoencoder (Kingma & Welling, 2014) and a variety of equivalent models introduced at the same time. The idea in

these models is to train an autoencoder whose latent representation satisfies certain distributional properties, which makes it easy to sample from the hidden variables, as well as from the data distribution (by plugging samples into the decoder).

The second are models based on adversarial sampling (Goodfellow et al., 2014). This approach forgoes the need to encourage a particular latent distribution, and in fact an encoder altogether, by training a simple feed-forward neural network to generate “data-like” examples. “Data-likeness” is judged by a simultaneously trained, but otherwise separate, discriminator neural network.

For both types of approach, sequential variants were introduced recently, which were shown to work much better in terms of visual quality: The DRAW network (Gregor et al., 2015), for example, is a sequential version of the variational autoencoder, where images are generated by accumulating updates into a canvas using a recurrent network. This also allows the use of an attention mechanism which was shown to be a crucial factor to obtain good samples. As the sequential variant of an adversarial network, the LAPGAN model (Denton et al., 2015) generates images in coarse-to-fine fashion, by generating and upsampling in multiple steps.

Motivated by the successes of sequential generation, in this paper, we propose a new image generation model based on a recurrent network. Like (Denton et al., 2015), our model generates an image in a sequence of structurally identical steps, but in contrast to that work we do not impose a coarse-to-fine (or any other) structure on the generation procedure. Instead we let the recurrent network learn the optimal procedure by itself. In contrast to (Gregor et al., 2015), we obtain very good samples without resorting to an attention mechanism and without variational training criteria (such as a KL-penalty on the hiddens).

Our model is mainly inspired by a third type of image generation method proposed recently by (Gatys et al., 2015). In this work, the goal is to change the texture (or “style”) of a given reference image by generating a new image that

matches image features and texture features within the layers of a pretrained convolutional network. As shown by (Gatys et al., 2015), ignoring the style- cost in this approach and only matching image features, it is possible to render images which are similar to the reference image. As we shall present, unrolling the gradient descent based optimization that generates the target image yields a recurrent computation, in which an “encoder” convolutional network extracts images of the current “canvas”. The resulting code and the code for the reference image get fed into a “decoder” which decides on an update to the “canvas”.

This view, along with the successes of trained sequential generation networks, suggests that an “iteratively stepped” convolutional network trained to accumulate updates onto a visual canvas, should be good at generating images in general, not just those shown as reference images. We show in this paper that this indeed is the case.

To evaluate and compare the relative performance of adversarial generative models quantitatively, we also introduce a new evaluation scheme based on a “cross-over” battle between the discriminators and generators of the two models.

## 2. Background

Generative Adversarial Networks (GAN) are built upon the concept of *game theory*, where two models play a non-cooperative game (Nash, 1951). The game is between a generative and a discriminative model,  $G$  and  $D$ , respectively, such that the generative model generates samples that are hard for the discriminator  $D$  to distinguish from real data, and the discriminator tries to avoid getting fooled by the generative model  $G$ .

Formally, the discriminative model is a classifier  $D : \mathbb{R}^M \rightarrow \{0, 1\}$  that tries to differentiate whether a given point  $\mathbf{x} \in \mathbb{R}^M$  came from the data or not. The generative model  $G : \mathbb{R}^K \rightarrow \mathbb{R}^M$  generates samples  $\mathbf{x} \in \mathbb{R}^M$  that are indistinguishable from the data by mapping a sample  $\mathbf{z} \in \mathbb{R}^K$  drawn randomly from some prior distribution  $p(\mathbf{z})$  to the data space. These models can be trained by playing a *minmax game* as follows:

$$\min_{\theta_G} \max_{\theta_D} V(D, G) = \min_{\theta_G} \max_{\theta_D} \left[ \mathbb{E}_{\mathbf{x} \sim p_D} [\log D(\mathbf{x})] + \mathbb{E}_{\mathbf{z} \sim p_G} [\log (1 - D(G(\mathbf{z})))] \right]. \quad (1)$$

where  $\theta_G$  and  $\theta_D$  are the parameters of discriminator and generator, respectively.

In practice, the second term in Equation 1 is troublesome due to the saturation of  $\log(1 - D(G(\mathbf{z})))$ . This makes insufficient gradient flow through the generative model  $G$  as the magnitude of gradients get smaller and prevent them from learning. To remedy the vanishing gradient problem,

the objective function in Equation 1 is reformulated into two separate objectives:

$$\begin{aligned} \max_{\theta_D} \mathbb{E}_{\mathbf{x} \sim p_D} [\log D(\mathbf{x})] + \mathbb{E}_{\mathbf{z} \sim p_G} [\log (1 - D(G(\mathbf{z})))] \\ + \max_{\theta_G} \mathbb{E}_{\mathbf{z} \sim p_G} [\log D(G(\mathbf{z}))]. \end{aligned} \quad (2)$$

Although Equation 2 is not the same as Equation 1, the underlying intuition is the same. Moreover, the gradient of generators for the two different objectives are always pointing in the same direction and the two objectives have the same fixed points.

The generating and discriminating procedure are simple. Let us consider a prior distribution to be a Gaussian distribution with zero-mean and unit variance. Then, the process of generating an output is simply to pass a sample  $\mathbf{z} \sim \mathcal{N}(\mu = 0, \sigma = 1)$  to the generative model to obtain the sample  $\mathbf{x} \sim G(\mathbf{z}; \theta_G)$ . Note that the generative model  $G$  can be a deterministic or a probabilistic model. However, only deterministic models have been deployed in the past, which makes  $\mathbf{x} = G(\mathbf{z}; \theta_G)$ . Subsequently, the sample can be passed on to the discriminator to predict  $D(\mathbf{x}; \theta_D)$ .

After computing the cost in Equation 2, the model parameters can be updated through backpropagation. Due to the two different min-max operators in Equation 2, the update rule is set as follows:

$$\{\theta'_D, \theta'_G\} \leftarrow \begin{cases} \text{Update } \theta_D & \text{if } D(\mathbf{x}) \text{ predicts wrong} \\ \text{Update } \theta_D & \text{if } D(G(\mathbf{z})) \text{ predicts wrong} \\ \text{Update } \theta_G & \text{if } D(G(\mathbf{z})) \text{ predicts correct} \end{cases}$$

Ideally, we would like our generative model to learn a distribution such that  $p_G = p_D$ . This requires the generative model to be capable of transforming a simple prior distribution  $p(\mathbf{z})$  to more complex distributions. In general, deep neural networks are good candidates as they are capable of modeling complicated functions and they were shown to be effective in previous works (Goodfellow et al., 2014; Mirza & Osindero, 2014; Gauthier, 2014; Denton et al., 2015). However, note that this min-max continuous game does not necessarily have a Nash equilibrium solution because there are uncountably many possible neural networks.

Recently, (Radford et al., 2015) showed excellent samples of realistic images using fully convolutional neural network as the discriminative model and fully deconvolutional neural network (Zeiler et al., 2011) as the generative model. Then, the  $l^{th}$  convolutional layer in the discriminative network takes the form

$$h_j^{k(l)} = f \left( \sum_{j \in M_k} h_j^{l-1} * W^{k(l)} + b_j^{k(l)} \right), \quad (3)$$

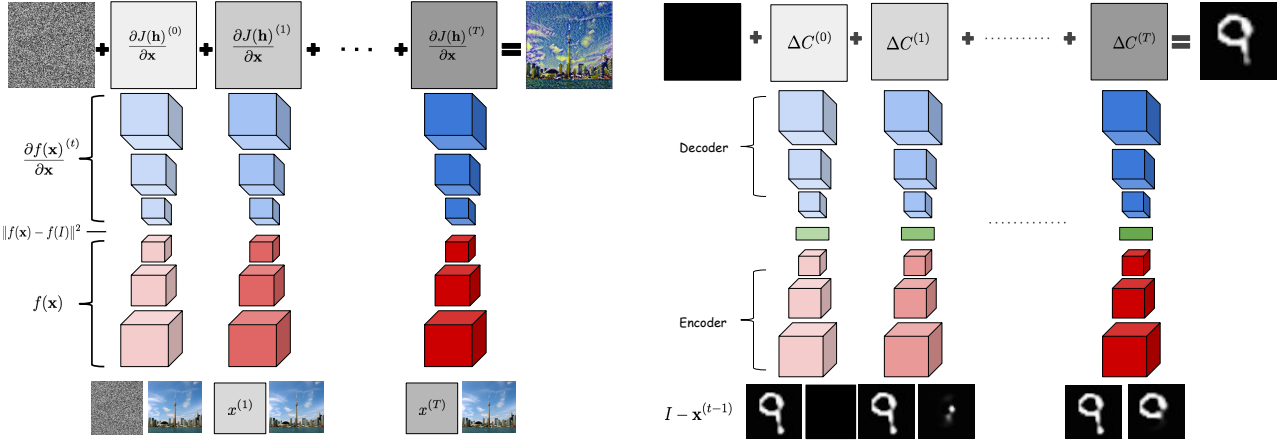


Figure 1. **Left:** Unrolling the gradient-based optimization of pixels in Gatys et al. **Right:** The DRAW network.

and the  $l^{th}$  convolutional transpose layer<sup>1</sup> in the generative network takes the form

$$g_j^{c(l)} = f \left( \sum_{j \in M_c} g_j^{l-1} \star W^{c(l)} + b_j^{c(l)} \right). \quad (4)$$

In these equations,  $\star$  is the convolution operator,  $\star$  is the convolutional transpose operator,  $M_j$  is the selection of inputs from the previous layer (“input maps”),  $f$  is an activation function, and  $\{W^{k(l)}, b_j^{k(l)}\}$  and  $\{W^{c(l)}, b_j^{c(l)}\}$  are the parameters of the discriminator and generator at layer  $l$ . The detailed explanation of convolutional transpose is explained in the supplementary materials.

The quality of samples can depend on several tricks (Radford et al., 2015), including: 1. Removing fully connected hidden layers and replacing pooling layers with strided convolutions on the discriminator (Springenberg et al., 2014) and fractional-strided convolutions (upsampling) on the generator. 2. Using batch normalization (Ioffe & Szegedy, 2015) on both generative and discriminative models. 3. Using ReLU activations in every layer of the generative model except the last layer, and using LeakyReLU activations (Maas et al., 2013) in all layers of the discriminative model. Overall, these architectural tricks make it easier to generate smooth and realistic samples. In the following section, we rely on some of these tricks and incorporate them in our proposed model as well.

### 3. Model

Here, we propose sequential modeling using GANs on images. Before introducing our proposed methods, we discuss some of the motivations for our approach. One inter-

<sup>1</sup>It is more proper to say “convolutional transpose operation” rather than “deconvolutional” operation. Hence, we will be using the term “convolutional transpose” from now on.

esting aspect of models such as the Deep Recurrent Attentive Writer (DRAW) (Gregor et al., 2015) and the Laplacian Generative Adversarial Networks (LAPGAN) (Denton et al., 2015) are that they generate image samples in a sequential process, rather than generating them in one shot. Both were shown to outperform their ancestor models, which are the variational auto-encoder (Kingma & Welling, 2014) and GAN, respectively. The obvious advantage of such sequential models is that repeatedly generating outputs conditioned on previous states simplifies the problem of modeling complicated data distributions by mapping them to a sequence of simpler problems.

There is a close relationship between sequential generation and *Backpropagating to the Input* (BI). BI is a well-known technique where the goal is to obtain a neural network *input* that minimizes a given objective function derived from the network. For example, (Gatys et al., 2015) recently introduced a model for stylistic rendering by optimizing the input image to simultaneously match higher-layers features of a *reference content image* and a non-linear, texture-sensitive function of the same features of a *reference style image*. They also showed that in the absence of the style-cost, this optimization yields a rendering of the content image (in a quality that depends on the chosen feature layer).

Interestingly, rendering by feature matching in this way is itself closely related to DRAW (Gregor et al., 2015): optimizing a matching cost with respect to the input pixels with backprop amounts to first extracting the current image features  $f_x$  at the chosen layer using a forward path through the network (up to that layer). Computing the gradient of the feature reconstruction error then amounts to back-propagating the difference  $f_x - f_I$  back to the pixels. This is equivalent to traversing a “decoder” network, defined as the linearized, inverse network that computes the backward pass. The negative of this derivative is then added into the current version,  $x$ , of the generated image.

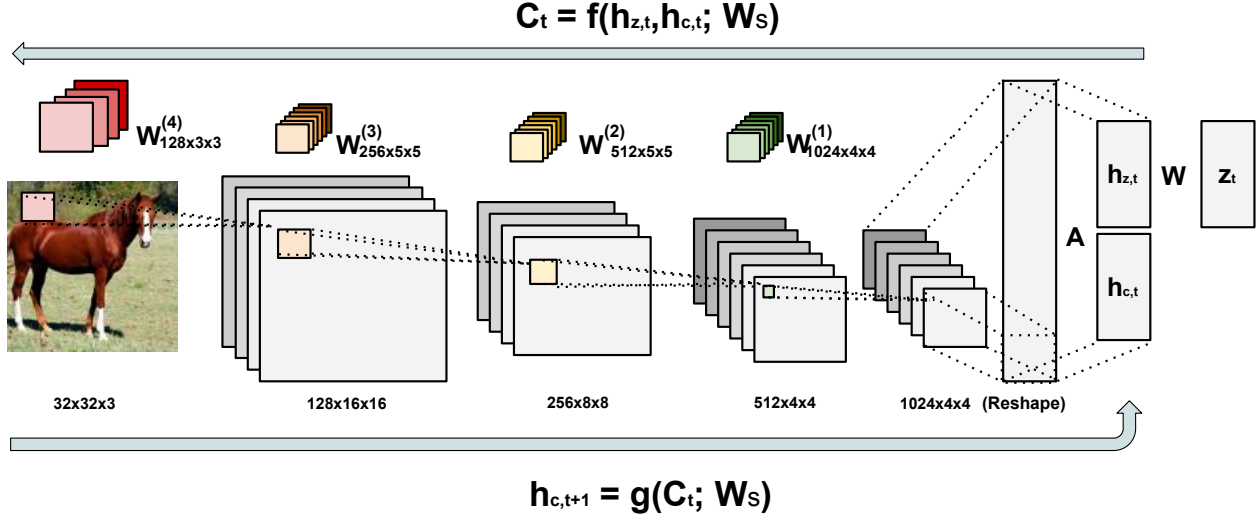


Figure 2. Depiction of single time step component of Generative Recurrent Adversarial Networks architecture layed out. (The numbers of the figures are used for modelling CIFAR10 dataset)

We can thus think of the image  $x$  as a buffer or ‘‘canvas’’ onto which updates are accumulated sequentially (see the left of Figure 1). Like in the DRAW model, the updates are computed using a (forward) pass through an encoder network, followed by a (backward) pass through a decoder network. This approach is almost identical to the DRAW network, except for three subtle differences (see, (Gregor et al., 2015)): (i) in DRAW, the difference between the current image and the image to be rendered is used in the forward pass, whereas here this difference is computed in the feature space (after encoding); (ii) in DRAW the decoder is nonlinear; (iii) DRAW uses a learned, attention-based decoder and encoder rather than (fixed) convolutional network. (see the right of Figure 1) We thoroughly elaborate the relationship between the two methods in the supplementary material.

In this work, we explore a *generative recurrent adversarial network* as an intermediate between DRAW and gradient-based optimization based on a generative adversarial objective function

### 3.1. Generative Recurrent Adversarial Networks

The underlying structure of a Generative Recurrent Adversarial Networks (GRAN) is similar to other GANs. The main difference between GRAN versus other generative adversarial models is that the generator  $G$  consists of a recurrent feedback loop that takes a sequence of noise samples drawn from the prior distribution  $\mathbf{z} \sim p(\mathbf{z})$  and draws the output at different time steps  $\Delta C_1, \Delta C_2, \dots, \Delta C_T$ . Figure 3 delineates the high-level abstraction of GRAN.

At each time step  $t$ , a sample  $\mathbf{z}$  from the prior distribution

is passed onto a function  $f(\cdot)$  with the hidden state  $\mathbf{h}_{c,t}$  where  $\mathbf{h}_{c,t}$  represents the current encoded status of the previous drawing  $\Delta C_{t-1}$ .  $\Delta C_t$  is what is drawn to the canvas at time  $t$  and it contains the output of the function  $f(\cdot)$ . (See Figure 2.) More specifically,  $\mathbf{h}_{c,t}$  is a hidden state that is encoded by function  $g(\cdot)$  from the previous drawing  $\Delta C_{t-1}$ . Henceforth, the function  $g(\cdot)$  can be seen as a way to mimic the inverse of the function  $f(\cdot)$ . Accumulating the updates at each time step yields the final sample drawn to the canvas  $\mathcal{C}$ .

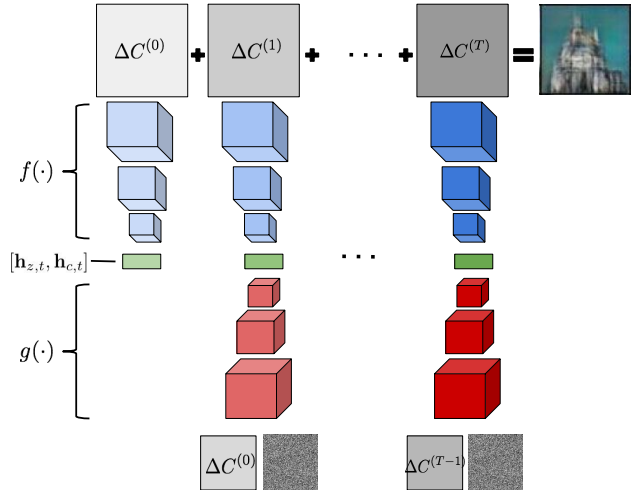


Figure 3. Abstraction of Generative Recurrent Adversarial Networks. The function  $f(\cdot)$  serves as the decoder and the function  $g(\cdot)$  serves as the encoder of GRAN.

Ultimately, the function  $f(\cdot)$  acts as a decoder that receives the input from the previous hidden state  $\mathbf{h}_{c,t}$  and noise sam-

ple  $\mathbf{z}$ , and the function  $g(\cdot)$  acts as an encoder that provides a hidden representation of the output  $\Delta C_{t-1}$  for time step  $t$ . One interesting aspect of GRAN is that the procedure of GRAN starts with a decoder instead of an encoder, whereas most of auto-encoding type of models such as VAE or DRAW start by encoding an image as shown in Figure 3.

In the following, we describe the details of the GRAN procedure more precisely. We have an initial hidden state  $\mathbf{h}_{c,0}$  where  $\mathbf{h}_{c,0}$  is set to the zero vector at the beginning. As well,  $\mathbf{h}_{z,0}$  and  $\mathbf{z}$ <sup>2</sup> are initialized as such

$$\mathbf{z} \sim p(Z) \quad (5)$$

$$\mathbf{h}_{z,0} = \tanh(W\mathbf{z} + \mathbf{b}). \quad (6)$$

Then, we compute the following for each time step from  $1 \dots T$ :

$$\mathbf{h}_{c,t} = g(\Delta C_{t-1}) \quad (7)$$

$$\Delta C_t = f([\mathbf{h}_{z,t}, \mathbf{h}_{c,t}]), \quad (8)$$

where  $[\mathbf{h}_{z,t}, \mathbf{h}_{c,t}]$  denotes the concatenation of two vector  $\mathbf{h}_{z,t}$  and  $\mathbf{h}_{c,t}$ . At the end, we sum all the drawings and then apply the logistic function to the sum in order to scale the final output to be in between  $(0, 1)$  such that

$$\mathcal{C} = \sigma\left(\sum_{t=1}^T \Delta C_t\right). \quad (9)$$

The reason for applying the affine transformation along with  $\tanh(\cdot)$  function in Equation 6 is to rescale  $\mathbf{z}$  to  $(-1, 1)$  so that it lies in the same (bounded) domain as  $\mathbf{h}_{c,t}$ ;  $g(\cdot)$  applies  $\tanh(\cdot)$  at the end, which makes  $\mathbf{h}_{c,t}$  also to be in the range of  $(-1, 1)$ .

In general, one can declare the function  $f(\cdot)$  and  $g(\cdot)$  to be any type of model. We used a variant of DCGAN (Radford et al., 2015) in our experiments. Figure 2 demonstrates the architecture of GRAN at time step  $t$ . The function  $f(\cdot)$  starts with one fully connected layer at the bottom and deconvolutional layers with fractional-stride convolution at rest of the upper layers. Conversely, the function  $g(\cdot)$  starts from convolutional layers and the full connected layer at the top. The architecture between two functions,  $f(\cdot)$  and  $g(\cdot)$  is symmetric as shown in Figure 3. The overall network is trained via backpropagation through the time.

<sup>2</sup>Note that we explore two scenarios of sampling  $\mathbf{z}$  in the experiments. The first scenario is where  $\mathbf{z}$  is sampled once in the beginning, then  $\mathbf{h}_{z,t} = \mathbf{h}_{z,0}$  as consequence, and another scenario is where  $\mathbf{z}$  is sampled at every time step.

## 4. Model Evaluation: Battle between GANs

A problem with generative adversarial models is that there is not a clear way to evaluate them quantitatively. In the past, (Goodfellow et al., 2014) evaluated GANs by looking at the single nearest-neighbour data from the generated samples. LAPGAN was evaluated in the same way, as well as using human inspections (Denton et al., 2015). For human inspections, volunteers were asked to judge whether given images are drawn from the dataset or generated by LAPGAN. In that case, the discriminator can be viewed as a human, while the generator is a trained GAN. The problems with this approach are that human inspectors may have high variance, which makes it necessary to average over a large number of human inspectors, and the experimental setup is both expensive and cumbersome. A third evaluation scheme, used recently by (Radford et al., 2015) is classification performance. However, this approach is rather indirect and relies heavily on the choice of classifier. For example, in mentioned work they used the nearest neighbour classifier, which suffers from the problem that Euclidean distance is not a good dissimilarity measure for images.

Here, we propose an alternative way to evaluate generative adversarial models. Our approach is to directly compare two generative adversarial models by having them engage in a “battle” against each other. The naive intuition is that because every generative adversarial models consist of a discriminator and a generator in pairs, we can exchange the pairs and have them play the generative adversarial game against each other. Figure 5 illustrate this approach<sup>3</sup>.

The training and test stage are as follows. Consider two generative adversarial models,  $M_1$  and  $M_2$ . Each model consists of a generator and a discriminator,

$$M_1 = \{(G_1, D_1)\} \text{ and } M_2 = \{(G_2, D_2)\}. \quad (10)$$

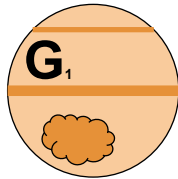
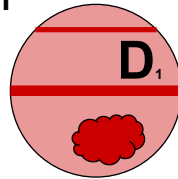
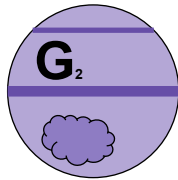
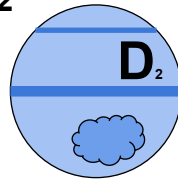
During the training stage, both models are being trained to prepare them for the battle with one another. Thus, in the training phase,  $G_1$  competes with  $D_1$  in order to be equipped for the battle in the test phase. Likewise for  $G_2$  and  $D_2$ . In the test phase, model  $M_1$  plays against model  $M_2$  by having  $G_1$  try to fool  $D_2$  and vice-versa.

Table 1. Model Comparison Metric for GANs

	$M_1$	$M_2$
$M_1$	$D_1(G_1(\mathbf{z}))$ , $D_1(\mathbf{x}_{train})$	$D_1(G_2(\mathbf{z}))$ , $D_1(\mathbf{x}_{test})$
$M_2$	$D_2(G_1(\mathbf{z}))$ , $D_2(\mathbf{x}_{test})$	$D_2(G_2(\mathbf{z}))$ , $D_2(\mathbf{x}_{train})$

Accordingly, we end up with the combinations shown in Table 1. Each entry in the table contains two scores, one

<sup>3</sup>Larger figure shown in the supplementary materials.

**Training Phase****M1****M2****Figure 4.** Training Phase of Generative Adversarial Networks.

from discriminating training or test data points and the other from discriminating generated samples. At test time, we can look at the following ratios between the discriminative scores of the two models:

$$r_{test} \stackrel{\text{def}}{=} \frac{\epsilon(D_1(\mathbf{x}_{test}))}{\epsilon(D_2(\mathbf{x}_{test}))} \text{ and} \quad (11)$$

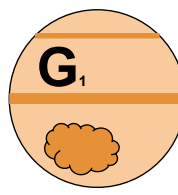
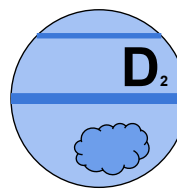
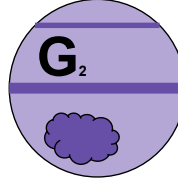
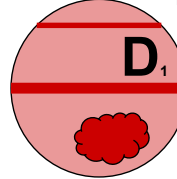
$$r_{sample} \stackrel{\text{def}}{=} \frac{\epsilon(D_1(G_2(\mathbf{z})))}{\epsilon(D_2(G_1(\mathbf{z})))}, \quad (12)$$

where  $\epsilon(\cdot)$  outputs the classification error rate. These ratios allow us to compare the model performance.

The test ratio,  $r_{test}$ , tells us which model generalizes better since it is based on discriminating the test data. Note that when the discriminator is overfitted to the training data, the generator will also be affected by this. This would increase the chances of producing biased samples towards the training data.

The sample ratio,  $r_{sample}$ , tells us which model can fool the other model more easily, since the discriminators are classifying over the samples generated by their opponents. Strictly speaking, as our goal is to generate good samples, the sample ratio determines which model is better at generating good (“data like”) samples. We suggest using the sample ratio to determine the winning model, and to use the test ratio to determine the validity of the outcome as outlined below.

The reason for using the latter is due to the occasional possibility of the sample ratio being biased. Hence, the fairness of the battle dissipates when the winner is solely determined by the sample ratio. This is because, computing the sample ratio requires discriminators from each model, and it is possible that one of the discriminators are biased towards the training data more so than the other (i.e. overfitted on the training data). In order to address this issue,

**Test Phase (a.k.a Battle Phase)****M1 versus M2****Figure 5.** Training Phase and Test Phase of Generative Adversarial Networks.

our proposed evaluation metric qualifies the sample ratio to be judged by the test ratio as follows:

$$\text{winner} = \begin{cases} \text{M1} & \text{if } r_{sample} < 1 \text{ and } r_{test} \simeq 1 \\ \text{M2} & \text{if } r_{sample} > 1 \text{ and } r_{test} \simeq 1 \\ \text{Not Applicable} & \text{otherwise} \end{cases} \quad (13)$$

Basically, we impose a condition where  $r_{test} \simeq 1$ . This assures that none of the discriminator is overfitted more than the other. If  $r_{test} \neq 1$ , then this implies that  $r_{sample}$  is biased, and thus, the sample ratio is no longer applicable.

This evaluation is called, Generative Adversarial Metric (GAM). GAM is not only able to compare generative adversarial models against each other, but also able to partially compare other models, such as the VAE or DRAW. This is done by observing the error rate of GRAN’s discriminators based on the samples of other generative model as a evaluation criterion. For example, we reported the error rates of the GRAN’s discriminators with the samples of VAEs, i.e.  $err(D(\mathbf{z}))$  where  $\mathbf{z}$  are the samples of DVAE and  $D(\cdot)$  is the discriminator of GRAN.

**5. Experiments**

In order to evaluate whether the extension of sequential generation enhances the performance, we assessed both quantitatively and qualitatively under three different image datasets. We conducted several empirical studies on GRAN under the model selection metrics discussed in Section 4. Additionally, we observed generated samples and analyzed them to evaluate the GRAN qualitatively.

The **MNIST dataset** contains 60,000 images for training and 10,000 images for testing and each of the images is 28×28 pixels for handwritten digits from 0 to 9 (LeCun et al., 1998). Out of the 60,000 training examples, we

Table 2. Model Evaluation on various data sets.

DATA SET	BATTLER	TEST RATIO	SAMPLE RATIO	WINNER
MNIST	GRAN1 vs. GRAN3	0.79	1.75	GRAN3
	GRAN1 vs. GRAN5	0.95	1.19	GRAN5
CIFAR10	GRAN1 vs. GRAN3	1.28	1.001	GRAN3
	GRAN1 vs. GRAN5	1.29	1.011	GRAN5
	GRAN3 vs. GRAN5	1.00	2.289	GRAN5
LSUN	GRAN1 VS. GRAN3	0.95	13.68	GRAN3
	GRAN1 vs. GRAN5	0.99	13.97	GRAN5
	GRAN3 vs. GRAN5	0.99	2.38	GRAN5



Figure 6. MNIST Samples generated by GRAN

used 10,000 examples as validation set to tune the hyper-parameters of our model.

**The CIFAR10 dataset** consists of 60000 32×32 colour images in 10 classes, with 6000 images per class. There are 50000 training images and 10000 test images.

**The LSUN dataset** consists of high resolution natural scene images with 10 different classes (Yu et al., 2015). We considered training on outdoor church images, which contains 126,227 training, 300 validation, and 1000 test images. These images were downsampled to 64×64 pixels.

All datasets were normalized such that each pixel value ranges in between [0, 1]. For all of our results, we optimized the models with ADAM (Kingma & Ba, 2014). The batch size was set to 100, and the learning rate was selected from a discrete range chosen based on the validation set. Importantly, we used different learning rates for the discriminative network and generative network. Throughout the experiments, we found that having different learning rates is useful to obtain successfully trained generative adversarial models. As our proposed model is a sequential

Table 3. Comparison between GRAN and non-adversarial models on MNIST.

BATTLER	ERROR
GRAN1 vs. DVAE	0.058
GRAN3 vs. DVAE	0.01
GRAN1 vs. DRAW	0.347
GRAN3 vs. DRAW	0.106

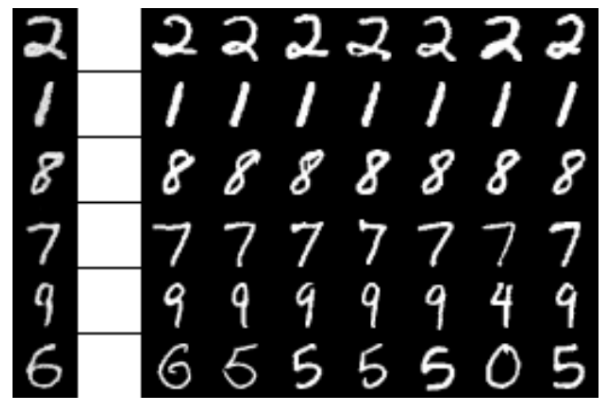


Figure 7. Nearest Neighbour training examples for MNIST samples.



Figure 8. Drawing at different time steps on mnist samples.

generator, we must select the number of steps,  $T$ , to run the model for generation. We compared the models in different number of timesteps,  $\{1, 3, 5\}$ . Note that GRAN is equivalent to DCGAN when  $T = 1$  up to one extra fully connected layer. We denote this as GRAN1.

Throughout the experiments, we used a similar architecture for the generative and discriminative network as shown in Figure 2 and Figure 3. The convolutional layers of the networks for the discriminator and generator are shared. The number of convolutional layers and the number of hidden units at each layer were varied based on the dataset. Table 4 shows the number of convolution kernels and the size of the filters at each convolutional layer. The numbers in the array from left to right corresponds to each bottom to top layer of the convolutional neural network. One can tie the weights



Figure 9. CIFAR10 samples generated by GRAN



Figure 10. Samples of LSUN images generated by GRAN

of convolutional and convolutional transpose in the encoder and decoder of GRAN to have the same number of parameters for both DCGAN and GRAN.<sup>4</sup> In the following, we

Table 4. The experimental hyper-parameters on different data sets.

DATASET	# KERNELS	FILTER SZ.	# z
MNIST	[80, 40, 1]	[5,5,5]	60
CIFAR10	[1024, 512, 216, 3]	[5,5,5,5]	100
LSUN	[1024, 512, 216, 128, 3]	[5,5,5,5,5]	100

analyze the results by answering a set of questions on our experiments.

*Q: How does GRAN perform?*

The performance of GRAN is presented in Table 2. We focused on comparing GRANs with 1, 3 and 5 time steps, which were denoted as GRAN1, GRAN3 and GRAN5. For all three datasets, GRAN3 and GRAN5 outperformed GRAN1 as shown in Table 2.

*Q: How do GRAN and other GAN type of models perform compared to non generative adversarial models?*

Although this may not be the best way to assess the two models since generator of GRAN does not get assessed explicitly, we tested comparing our model to other generative models such as denoising VAE (DVAE) (Im et al., 2015)

and DRAW on the MNIST dataset. Table 3 presents the results of applying GAM as described in the end of Section 4. The error rates were all below 50%, and especially low for DVAE’s samples. Surprisingly, even though samples from DRAW look very nice, the error rate on their samples were also quite low with GRAN3. This illustrate that the discriminator of generative adversarial models are good at discriminating the samples generated by DVAE and DRAW. Our hypothesis is that the samples look nicer due to the smoothing effect of having a mean-square error in their objective, but they do not capture all relevant aspects of the statistics of real handwritten images.

*Q: How do GRAN’s samples look?*

We present samples from GRAN for MNIST, cifar10 and LSUN in Figure 6, Figure 9 and Figure 10. Most of the MNIST and cifar10 samples shown in Figure 6 and Figure 9 appear to be discernible and reasonably classifiable by humans. Similarly, the LSUN samples from Figure 10 seem to cover variety of church buildings and contain fine detailed textures. The “image statistics” of two real image datasets are embedded into both types of sample.

*Q: Does GRAN overfit to the training data?*

Since it is infeasible to look across the training data and determine whether a given sample looks like a training case, it is common (albeit somewhat questionable) to look at  $k$ -nearest neighbours to do a basic sanity check. As shown in Figure 7, Figure 12, and Figure 11, one does not find any replicates of training data cases

<sup>4</sup>Code can be found at <https://github.com/jiwoongim/GRAN>

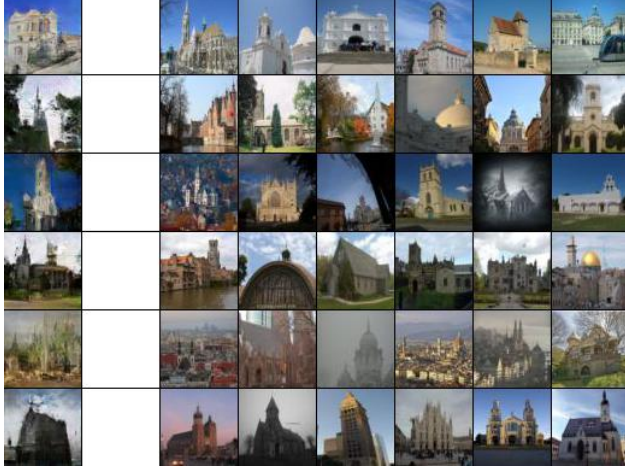


Figure 11. Nearest Neighbour training examples for lsun samples.

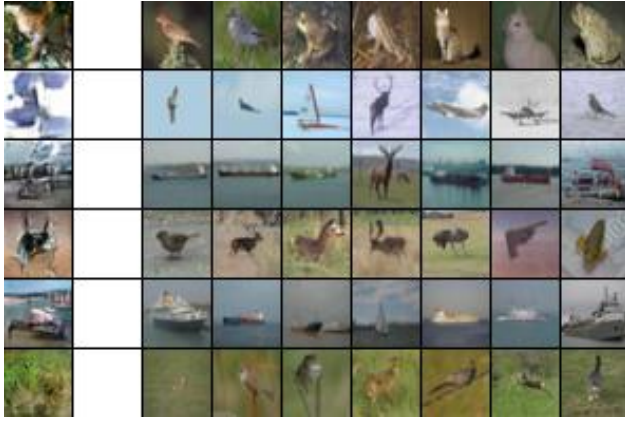


Figure 12. Nearest Neighbour training examples for cifar10 samples.

Empirically speaking, we did notice that GRAN tends to generate samples by interpolating between the training data. For example, Figure 11 in the supplementary material illustrates that the church buildings consist of similar structure of the entrance but the overall structure of the church is in a different shape. Based on such examples, we hypothesize that the overfitting for GRAN in the worst case may imply that the model learns to interpolate sensibly between training examples. This is not the typical way of the term overfitting is used for generative models, which usually refers to memorizing the data. In fact, in adversarial training in general, the objective function is not based on mean square error of the pixels which makes it not obvious how to memorize the training samples. However, this could mean that they will have a hard time generating images that are interpolated from test data.

*Q: How do the samples look like during the intermediate time steps  $t$ ?*



Figure 13. Drawing at different time steps on cifar10 samples.



Figure 14. Drawing at different time steps on lsun samples.



Figure 17. Drawing at different time steps on cifar10 samples with injecting different noises at every time step.

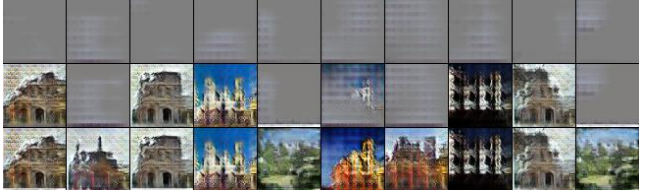


Figure 18. Drawing at different time steps on lsun samples with injecting different noises at every time step.

Figure 8, Figure 29, and Figure 35 present the intermediate samples when the total number of steps is 3. From the figures, we can observe the gradual development of the samples over time. The common observation from the intermediate samples is that images become more fine-grained and introduce details missing from the previous time step image. Intermediate samples for models with a total number of time steps of 5 can be found in the supplementary materials. This behaviour is somewhat similar to (Denton et al., 2015), as one might expect (although filling-in of color details suggest that there is more going on than just a coarse-to-fine behaviour). In general, this behaviour is not enforced in our case since we use an identical architecture at every time step.

*Q: What happens when we use different noise for each*

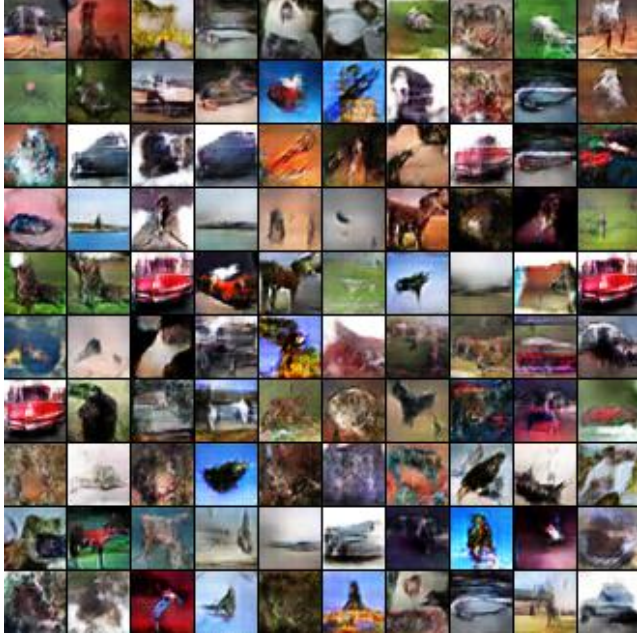


Figure 15. CIFAR10 samples generated by GRAN with injecting different noises at every time step?

Note that we sampled a noise vector  $\mathbf{z} \sim p(Z)$  and used the same noise for every time step. This is because  $\mathbf{z}$  acts as a reference frame in Artify as shown in Figure 1. On the other hand, DRAW injects different noise at each step,  $\mathbf{z}_1, \mathbf{z}_2, \dots, \mathbf{z}_T, \sim p(Z)$  due to variational auto-encoding properties. We also experimented with both sampling  $\mathbf{z}$  once in the beginning versus sampling  $\mathbf{z}_i$  at each time step. Here we describe the advantages and disadvantages to these two approaches.

For example, the samples of cifar10 and lsun generated by injecting different noises at each time step are shown in Figure 15 and Figure 16. Similar to when injecting same noise as shown in Figure 9 and Figure 10, the samples appear to be discernible and reasonably classifiable by humans as well. However, we observe few samples that look very close to each other. During the experiments, we found that when using different noise, it is more time consuming to find a set of hyper-parameters that produce good samples. Furthermore, the samples tend to collapse when training for a long time. Hence, we had to carefully select the total number of iterations. This illustrates that the training became much more difficult and it provokes GRAN to cheat by putting a lot of probability mass on samples that the discriminator cannot classify, which produce samples that looks very similar to each other.

On the other hand, when we look at the intermediate time steps of samples generated using multiple noises, we find that there are much more dynamics within each time step as



Figure 16. Samples of LSUN images generated by GRAN with injecting different noises at every time step

demonstrated in Figure 17 and Figure 18. For example, the colour of the train suddenly changed in Figure 17 and only the partial church is drawn in Figure 18. This illustrates that adding different noise increases the model capability on generating much dynamical images.

## 6. Discussion

We proposed a new generative model based on adversarial training of a recurrent neural network inspired by (Gatys et al., 2015). We showed conditions under which the model performs well and showed that it can produce higher quality visual samples than an equivalent single-step model. We also introduced a new metric for comparing adversarial networks quantitatively and showed that the recurrent generative model yields superior performance over existing state-of-the-art generative models under this metric.

## Acknowledgements

We thank the members of the LISA Lab at Montreal, in particular Mohammed Pezeshki and Donghyun Lee, for helpful discussions.

This research was developed with funding from the Defense Advanced Research Projects Agency (DARPA). The views, opinions, and/or findings expressed are those of the author and should not be interpreted as representing the official views or policies of the Department of Defense or the U.S. Government.

## References

Denton, Emily, Chintala, Soumith, Szlam, Arthur, and Fergus, Rob. Deep generative image models using a laplacian pyramid of adversarial networks. In *Proceedings of the Neural Information Processing Systems (NIPS)*, 2015.

Gatys, Leon A, Ecker, Alexander S, and Bethge, Matthias. A neural algorithm of artistic style. *arXiv preprint arXiv:1508.06576*, 2015.

Gauthier, Jon. Conditional generative adversarial nets for convolutional face generation. In *Class Project for Stanford CS231N: Convolutional Neural Networks for Visual Recognition, Winter semester 2014*, 2014.

Goodfellow, Ian J., Pouget-Abadie, Jean, Mirza, Mehdi, Xu, Bing, Warde-Farley, David, Ozair, Sherjil, Courville, Aaron, and Bengio, Yoshua. Generative adversarial nets. In *Proceedings of the Neural Information Processing Systems (NIPS)*, 2014.

Gregor, Karol, Danihelka, Ivo, Graves, Alex, Rezende, Danilo Jimenez, and Wierstra, Daan. Draw: A recurrent neural network for image generation. In *Proceedings of the International Conference on Machine Learning (ICML)*, 2015.

Hinton, Geoffrey E., Osindero, Simon, and Teh, Yee-Whye. A fast learning algorithm for deep belief nets. *Neural Computation*, 18(7):1527–1554, 2006.

Hyvriinen, Aapo, Hurri, Jarmo, and Hoyer, Patrick O. *Natural Image Statistics: A Probabilistic Approach to Early Computational Vision*. Springer Publishing Company, Incorporated, 1st edition, 2009. ISBN 1848824904, 9781848824904.

Im, Daniel Jiwong, Ahn, Sungjin, Memisevic, Roland, and Bengio, Yoshua. Denoising criterion for variational auto-encoding framework. In <http://arxiv.org/pdf/1509.00519.pdf>, 2015.

Ioffe, Sergey and Szegedy, Christian. Batch normalization: Accelerating deep network training by reducing internal covariate shift. In <http://arxiv.org/pdf/1502.03167.pdf>, 2015.

Kingma, Diederik and Ba, Jimmy. Adam: A method for stochastic optimization. In *Proceedings of the International Conference on Learning Representations (ICLR)*, 2014.

Kingma, Diederik P and Welling, Max. Auto-encoding variational bayes. In *Proceedings of the Neural Information Processing Systems (NIPS)*, 2014.

Maas, Andrew L, Hannun, Awsi Y, and Ng, Andrew Y. Rectifier nonlinearities improve neural network acoustic models. In *Proceedings of the International Conference on Machine Learning (ICML)*, 2013.

Mirza, Mehdi and Osindero, Simon. Conditional generative adversarial nets. In *Proceedings of the Neural Information Processing Systems Deep learning Workshop(NIPS)*, 2014.

Nash, John. Non-cooperative games. *The Annals of Mathematics*, 54(2):286–295, 1951.

Radford, Alec, Metz, Luke, and Chintala, Soumith. Unsupervised representation learning with deep convolutional generative adversarial networks. In <http://arxiv.org/pdf/1511.06434.pdf>, 2015.

Ranzato, Marc’Aurelio, Mnih, Volodymyr, Susskind, Joshua M, and Hinton, Geoffrey E. Modeling natural images using gated mrf. *Pattern Analysis and Machine Intelligence, IEEE Transactions on*, 35(9):2206–2222, 2013.

Springenberg, Jost Tobias, Dosovitskiy, Alexey, Brox, Thomas, and Riedmiller, Martin. Striving for simplicity: The all convolutional net. In <http://arxiv.org/abs/1412.6806>, 2014.

Yu, Fisher, Zhang, Yinda, Song, Shuran, Seff, Ari, and Xiao, Jianxiong. Lsun: Construction of a large-scale image dataset using deep learning with humans in the loop. In *arXiv:1506.03365 [cs.CV]* 10 Jun 2015, 2015.

Zeiler, Matthew D., Taylor, Graham W., and Fergus, Rob. Adaptive deconvolutional networks for mid and high level feature learning. In *International Conference on Computer Vision*, 2011.

## Supplementary Materials

### Additional Notes on Convolutional Transpose

In the following, we describe the convolutional transpose procedure in detail. For simplicity, let us consider the case of a 1-dimensional convolutional operation with one kernel and stride of 1:

$$o = i * W, \quad (14)$$

where  $i$  is an input,  $o$  is an output, and  $*$  is the convolution operator. Figure 19 and Figure 20 show an illustration of the 1D convolution.

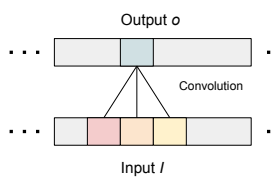


Figure 19. Applying convolution at index  $j$ .

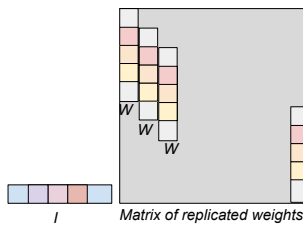


Figure 20. Convolution operation as a matrix operation.

Figure 19 presents the naive visualization of convolution over the input centered at index  $j$ , and Figure 20 presents the convolution operation in terms of matrix operation. The latter figure will be useful for understanding the convolutional transpose.

The gradient of Equation 17 wrt. the input takes the form

$$\frac{\partial o}{\partial i} = \frac{\partial i * W}{\partial i}. \quad (15)$$

Note that gradient of the convolution is a convolutional itself. This can be seen in Figure 21. We can re-express the *convolutional transpose*

$$\tilde{o} = \tilde{i} * W \quad (16)$$

where  $*$  is a convolutional transpose operator, and  $\tilde{o}$  and  $\tilde{i}$  are just input and output of the function.

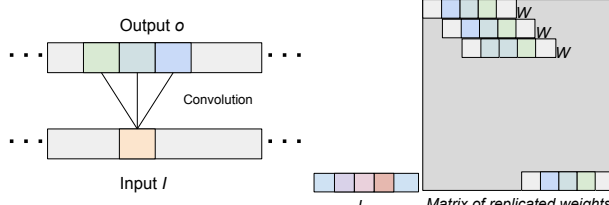


Figure 21. The gradient of convolution at index  $k$ .



Figure 22. Convolution operation as a matrix operations.

From Figure 22, we can observe that the gradient of convolutional formula in Equation 17 is just a transpose of the replicated input matrix.

Since the convolutional gradient uses the convolutional transpose operator, the convolutional transpose can be implemented by using the gradient.

Now we consider the case of strided convolution. For simplicity, we assume that the stride is 2. Similarly to before, we can write

$$o = i * W, \quad (17)$$

where  $i$  is an input,  $o$  is an output, and  $*$  is the convolution operator. Figure 23 and Figure 24 illustrate the 1D convolution.

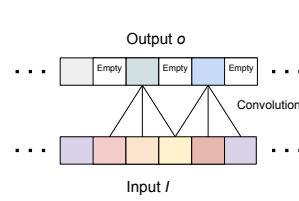


Figure 23. Applying convolution at index  $j$ .

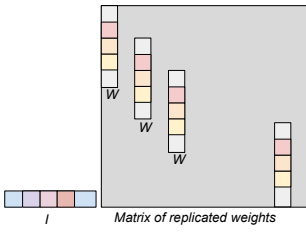


Figure 24. Stride Convolution operation as a matrix operations.

Figure 23 shows the visualization of 2-stride convolution over the input centered at index  $j$  and Figure 20 presents stride convolution operation in terms of a matrix operation.

The gradient of Equation 17 takes the form

$$\frac{\partial o}{\partial \hat{i}} = \frac{\partial \hat{i} * W}{\partial \hat{i}}. \quad (18)$$

where  $\hat{i}$  is the upsampled input  $i$  such that  $\hat{i} = [i_1, 0, i_2, 0, i_3, \dots, i_M, 0]$  for stride size equal to 2. Thus, the gradient of the strided convolution is a convolutional operation on an upsampled version of the input  $i$ . This can be observed from Figure 25.

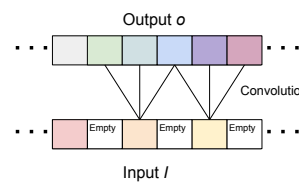


Figure 25. The gradient of convolution at index  $k$ .

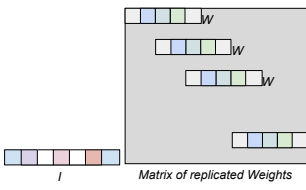


Figure 26. Convolution operation as a matrix operations. Overall, the convolutional transpose with strides is expressed as

$$\hat{o} = \hat{i} * W \quad (19)$$

where  $*$  is a convolutional transpose operator, and  $\hat{o}$  and  $\hat{i}$  are just input and output of the function.

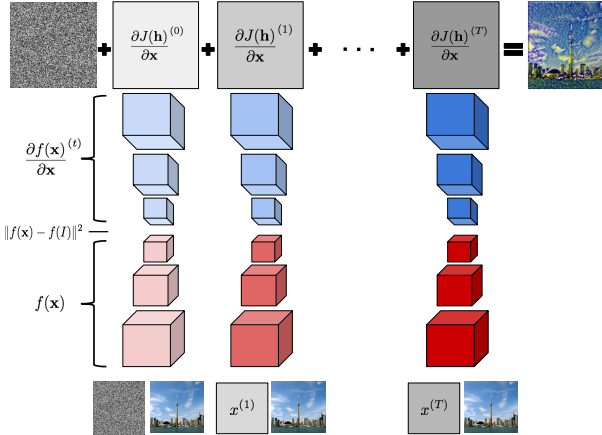


Figure 27. The gradient of convolution at index  $k$ .

### Relation between sequential modeling and backpropagating with respect to the input methods

We describe in more detail the relation between sequential modeling algorithms and backpropagation with respect to the input (BI). We will investigate their relation by examining a specific example.

The goal of BI is to find an optimal input by backpropagating an objective function with respect to the input. Let  $J(\mathbf{x})$  be a differentiable objective function that takes an input  $\mathbf{x}$ . Then, depending on whether the objective function is non-linear function or not, we iterate

$$\mathbf{x}_{opt} = \mathbf{x}^{(0)} - \sum_{t=1}^T \eta_t \frac{\partial J^{(t)}}{\partial \mathbf{x}^{(t-1)}} \quad (20)$$

where  $t$  denotes time, and the chain rule yields

$$\frac{\partial J^{(t)}}{\partial \mathbf{x}^{(t-1)}} = \frac{\partial J^{(t)}}{\partial f^{(t)}} \frac{\partial f^{(t)}}{\partial \mathbf{x}^{(t-1)}}, \quad (21)$$

where  $f(\cdot)$  is an intermediate function, which can be composed of many non-linear functions like neural networks, in the objective function  $J(\cdot)$ .

An example method that uses backpropagating with respect to the input is (Gatys et al., 2015). We will consider with only the content based objective of this method, and compare it to one of the well-known sequential generators, DRAW (Gregor et al., 2015). Figure 27 presents unrolled version. The objective function of BI is defined as  $\|f_{\mathbf{x}} - f_I\|^2$  where  $f_{\mathbf{x}}$  is the hidden representation of the input  $\mathbf{x}^{(t)}$  and  $f_I$  is the hidden representation of the *reference content image* of the pre-trained convolutional network  $f(\cdot)$ . The network layers are shown as red blocks. Furthermore, the blue blocks (or the upper half) the diagram in Figure 27 is the unrolled part of backpropagation gradient with respect to the input  $\frac{\partial f}{\partial \mathbf{x}}$ .

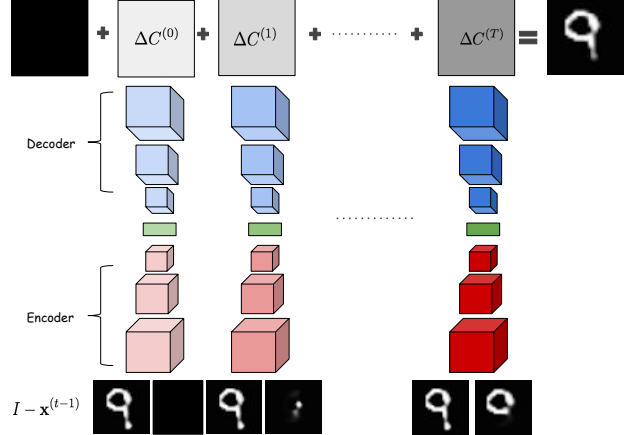


Figure 28. The abstract view of DRAW architecture is delineated.

The architecture of DRAW is shown in Figure 28<sup>5</sup>. DRAW takes the input and the difference between the input and canvas at time  $t$ , and it propagates through the encoder and decoder. At the end of each time step, DRAW outputs the updated canvas  $C^{(t)}$  by updating the previous canvas  $C^{(t-1)}$  with what will be drawn at time  $t$ , which is equivalent to change in the canvas  $\Delta C^{(t)}$ .

We can immediately notice the similarity between two architectures. The update procedure of draw, which is expressed as

$$C^{(t)} = C^{(t-1)} + \Delta C^{(t)}, \quad (22)$$

resembles the update rule of BI in Equation 20. Moreover, the encoder of DRAW,  $enc(\cdot)$ , can be seen as some function  $f(\cdot)$ , which will be the convolutional neural network in BI. Similarly, the decoder of DRAW,  $dec(\cdot)$ , can be seen as the unrolled version of BI, which corresponds to  $\frac{\partial f^{(t)}}{\partial \mathbf{x}^{(t-1)}}$ . The main difference is that BI takes the difference in the hidden representation space of  $f(\cdot)$  and DRAW takes the difference from the original input space.

Overall, we linked each components of two models by examining the abstraction as shown:

- $\Delta C^{(t)}$  reflects  $\frac{\partial J^{(t)}}{\partial \mathbf{x}^{(t-1)}}$ .
- $enc(\cdot)$  and  $dec(\cdot)$  reflect  $f(\cdot)$  and  $\frac{\partial f^{(t)}}{\partial \mathbf{x}^{(t-1)}}$ .

<sup>5</sup>The attention mechanism is omitted for clarity.

## Additional Supplementary Materials to the Experiments

**Analysis on GRAN samples** The following figure is to support the studies in the experiments, particularly it supports the description under *Q: Does GRAN overfit the training data?*.



Figure 29. Example of three different churches (samples) with some similarities.

## LSUN Samples for GRAN with time step equal to 3



Figure 30. Samples of LSUN images generated by GRAN5.

## Nearest Neighbor samples for GRAN with time step equal to 3



Figure 31. Nearest Neighbour training examples for cifar10 samples using GRAN5.

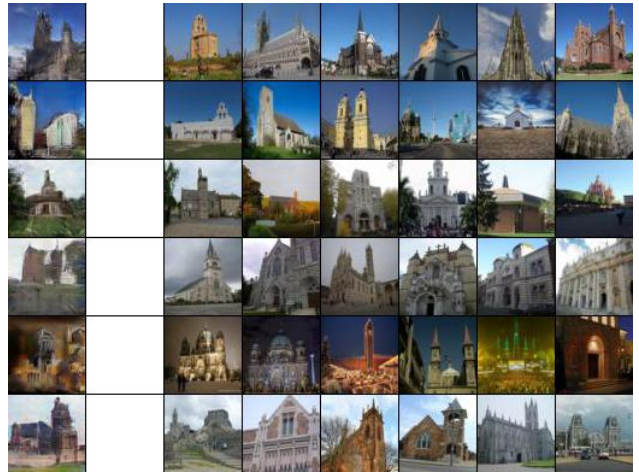


Figure 32. Nearest Neighbour training examples for lsun samples using GRAN5.

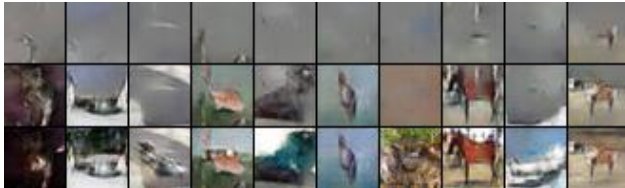
**Intermediate samples at time step equal to 3**


Figure 33. Drawing at different time steps on cifar10 samples.

**Intermediate samples at time step equal to 5**


Figure 34. Drawing at different time steps on cifar10 samples.



Figure 35. Drawing at different time steps on lsun samples.

**ImageNet samples**

We also trained GRAN on ImageNet dataset. ImageNet dataset (Deng et al., 2009) is a high resolution natural images. We rescaled the images to  $64 \times 64$  pixels. The architecture that was used for ImageNet is same as the architecture that was used for LSUN dataset except that there are three times more kernels on both generator and discriminator.

The samples are shown in Figure 36. Unfortunately, the samples do not generate objects from ImageNet dataset. However, it also shows that they are not overfitting, because they do not show actual objects but they are quite artistic. We hypothesize that this is because the model does not have

the capacity to model 1000 object classes. Hence, they stay as abstract objects.

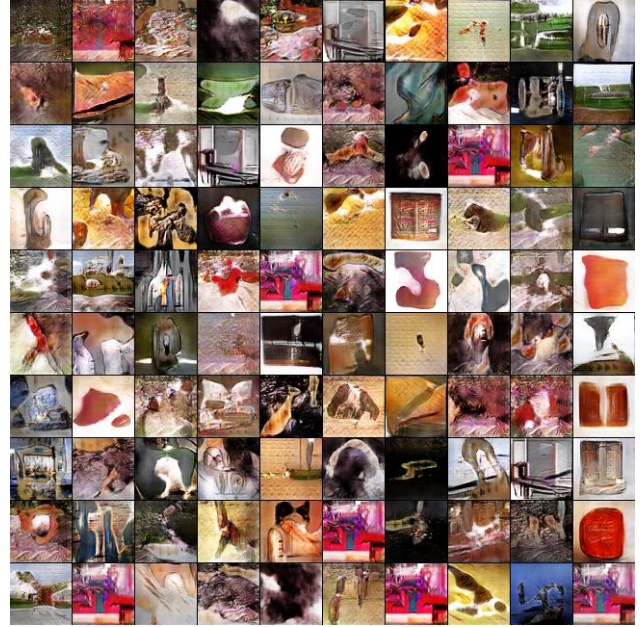


Figure 36. Samples of ImageNet images generated by GRAN3.